# Journal Pre-proof

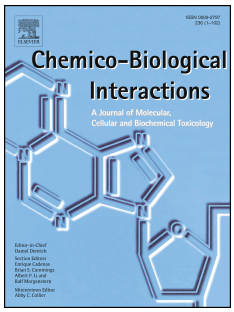


Plant isoquinoline alkaloids as potential neurodrugs: A comparative study of the effects of benzo[*c*]phenanthridine and berberine based compounds on β-amyloid aggregation

Daniela Marasco, Caterina Vicidomini, Pawel Krupa, Federica Cioffi, Pham Dinh Quoc Huy, Mai Suan Li, Daniele Florio, Kerensa Broersen, Maria Francesca De Pandis, Giovanni N. Roviello

PII: S0009-2797(20)31283-7

DOI: https://doi.org/10.1016/j.cbi.2020.109300

Reference: CBI 109300

To appear in: *Chemico-Biological Interactions*

Received Date: 23 July 2020

Revised Date: 17 September 2020

Accepted Date: 21 October 2020

Please cite this article as: D. Marasco, C. Vicidomini, P. Krupa, F. Cioffi, P.D. Quoc Huy, M. Suan Li, D. Florio, K. Broersen, M.F. De Pandis, G.N. Roviello, Plant isoquinoline alkaloids as potential neurodrugs: A comparative study of the effects of benzo[*c*]phenanthridine and berberine based compounds on β-amyloid aggregation, *Chemico-Biological Interactions* (2020), doi: https://doi.org/10.1016/j.cbi.2020.109300.

**Daniela Marasco:** conceptualization; investigation; data curation; writing – original draft ; **Caterina Vicidomini:** investigation; methodology; data curation; validation; **Pawel Krupa:** investigation; methodology; data curation; writing – original draft ;writing - review & editing **Federica Cioffi:** investigation; methodology **Pham Dinh Quoc Huy:** investigation; methodology **Mai Suan Li:** investigation; methodology; **Daniele Florio:** investigation; methodology **Kerensa Broersen:** investigation; methodology, writing – original draft; **Maria Francesca De Pandis:** conceptualization; writing – original draft; **Giovanni N. Roviello:** supervision; conceptualization; investigation; methodology; data curation; writing – original draft

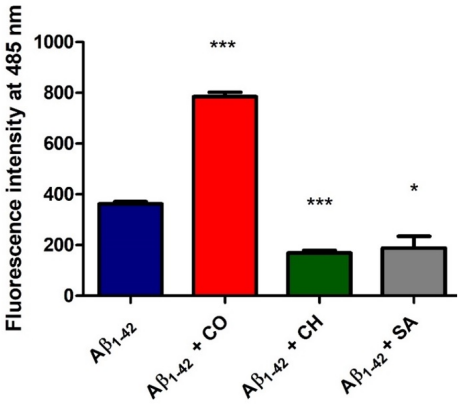


ThT fluorescence assay

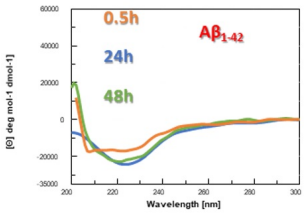


spectroscopy

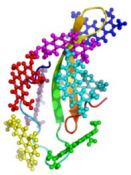

*in silico* studies

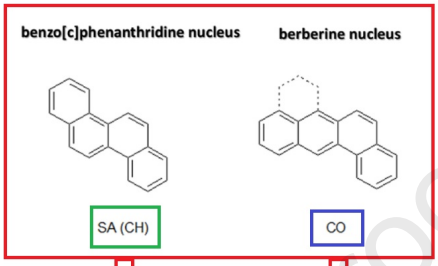


*docking studies*

*inhibit*

*increases*

*Aβ1-42 aggregation tendency*

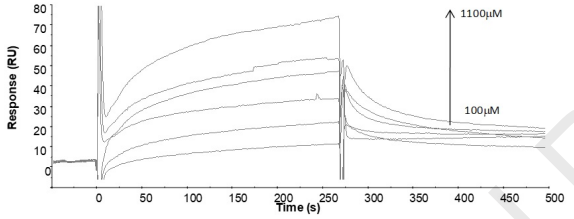


*SPR experiments*

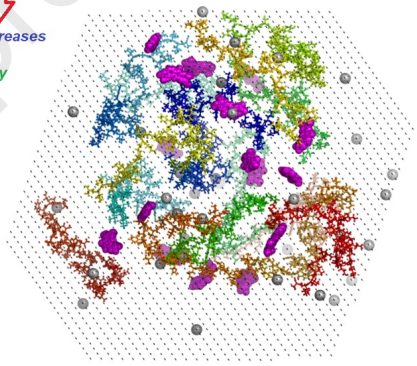

*Molecular Dynamics*

# Plant isoquinoline alkaloids as potential neurodrugs: a comparative study of the effects of benzo[*c*]phenanthridine and berberine based compounds on β-amyloid aggregation

**Daniela Marasco[a,b¶]; Caterina Vicidomini[b¶]; Pawel Krupa[c¶]; Federica Cioffi[d]; Pham Dinh Quoc Huy[c];Mai Suan Li[c,e]; Daniele Florio[a]; Kerensa Broersen[f]; Maria Francesca De Pandis[g]; Giovanni N. Roviello[b*]**

[a]Department of Pharmacy, University of Naples Federico II, Via Mezzocannone 16, 80134 Naples, Italy

[b]Istituto di Biostrutture e Bioimmagini IBB - CNR; Via Mezzocannone 16; I-80134 Naples, Italy

[c]Institute of Physics Polish Academy of Sciences, Al. Lotników 32/46, 02-668 Warsaw, Poland

[d]Nanobiophysics Group, Technical Medical Centre, Faculty of Science and Technology, University of Twente, Enschede, The Netherlands

[e]Institute for Computational Sciences and Technology, SBI building, Quang Trung Software City, Tan ChanhHiep Ward, District 12, Ho Chi Minh City, Vietnam

[f]Applied Stem Cell Technologies, Technical Medical Centre, Faculty of Science and Technology, University of Twente, Enschede, The Netherlands

[g]San Raffaele Cassino Institute, San Raffaele SPA, 03043 Cassino (FR), Italy

¶these authors equally contributed to this work.

*corresponding author; e-mail addresses: giroviel@unina.it; giovanni.roviello@cnr.it

**Abstract**

Herein we present a comparative study of the effects of isoquinoline alkaloids belonging to benzo[*c*]phenanthridine and berberine families on β-amyloid aggregation. Results obtained using a Thioflavine T (ThT) fluorescence assay and circular dichroism (CD) spectroscopy suggested that the benzo[*c*]phenanthridine nucleus, present in both sanguinarine and chelerythrine molecules, was directly involved in an inhibitory effect of $A\beta_{1-42}$ aggregation. Conversely, coralyne, that contains the isomeric berberine nucleus, significantly increased propensity for $A\beta_{1-42}$ to aggregate. Surface Plasmon Resonance (SPR) experiments provided quantitative estimation of these interactions: coralyne bound to $A\beta_{1-42}$ with an affinity ($K_D$=11.6 μM) higher than benzo[*c*]phenanthridines. Molecular docking studies confirmed that all three compounds are able to recognize $A\beta_{1-42}$ in different aggregation forms suggesting their effective capacity to modulate self-recognition mechanism. Molecular dynamics simulations indicated that coralyne increased the β-content of $A\beta_{1-42}$, in early stages of aggregation, consistently with fluorescence-based promotion of self-recognition mechanism by this alkaloid. At the same time, sanguinarine seemed to determine an increase of helical conformation corroborating its ability to delay aggregation as experimentally proved *in vitro*. Investigated compounds demonstrated to interfere with aggregation of $A\beta_{1-42}$ applying as starting leads in neurodegenerative diseases.

**Keywords**: amyloid beta; neurodrug; amyloid aggregation; natural products; chelerythrine; sanguinarine; coralyne; berberine

## 1. Introduction

Several neurodegenerative disorders, including Alzheimer's (AD), Parkinson's (PD) and Huntington's (HD) diseases are associated with aggregation of misfolded proteins [1, 2]. Among these, AD, a predominant cause of dementia worldwide [3, 4], is characterized by extracellular amyloid deposits, whose main component is the 42-amino acid amyloid β peptide ($A\beta_{1-42}$), and by intracellular neurofibrillary tangles composed of tau[5, 6].

$A\beta_{1–42}$ is a peptide cleaved from the amyloid precursor protein (APP), comprised of a charged *N*-terminal segment (amino acids 1–22), a hydrophobic central region (KLVFFA, amino acids 16–21), which alone is able to aggregate into insoluble fibrils, and a hydrophobic *C*-terminal region (residues 23–42). Once released as a monomer from APP into extracellular space, $A\beta_{1-42}$ undergoes a structural transition gaining β-sheet content, and tends to aggregate into oligomeric, protofibrillar and fibrillar species [7]. $A\beta_{1–42}$ oligomeric assemblies have been related to AD pathogenesis for their role in neuronal damage and neurotoxicity following $A\beta_{1–42}$ aggregation [8]. In this context, preventing $A\beta_{1–42}$ aggregation with small molecules is one of the prominent strategies for the development of new therapies for AD [9-11]. To this scope, several plant extracts and natural products, such as curcumin, epigallocatechin-3-gallate, and resveratrol, were evaluated with promising results [12-14]

Isoquinoline alkaloids (Figure 1) belong to one of the most complex families of plant alkaloids. They are nitrogenous metabolites distributed in many botanical families investigated nowadays for their significant biomedical importance[15-17]. Among these, benzo[*c*]phenanthridines and protoberberines are found in various vegetal sources belonging to the *Rutaceae* family (in particular from the *Zanthoxylum* genus [18]), with berberine (Figure 1) being an interesting candidate for PD

and AD thanks to multi-faceted defensive mechanisms and bio-molecular pathways involving this alkaloid [19, 20]. However, its use as a neurodrug is hampered by its cytotoxic effects at relatively high concentration [21]. Hence, a structurally modified version of berberine that results in the free hydroxyl-bearing Ber-D was prepared, which was found to inhibit the aggregation and cell toxicity of $A\beta_{1\text{-}42}$ *in vitro*[22]. The berberine nucleus in Ber-D comprises four rings, of which three aromatic, whereas the anti-leukemic berberine-like drug coralyne (here indicated as CO, Figure 1) contains all four aromatic rings[23, 24].

Other examples of plant isoquinoline alkaloids are sanguinarine (SA) and chelerythrine (CH, Figure 1), two tetracyclic aromatic compounds isolated from *Macleaya cordata* belonging to the family of benzo[*c*]phenanthridines, and also classifiable as azachrysenes[25, 26]. In particular, SA is endowed with several properties of therapeutic relevance, including the reduction of stress hormone levels as shown in studies carried out in animal models[27], of serum haptoglobin, and serum amyloid A (SAA) [27, 28]. This protein is mainly produced in the liver but also expressed extrahepatically in the central nervous system (CNS) [29], with increased levels in AD patients [29], and was recently recognized as a biomarker for COVID-19 [30], that is a recently-emerged viral disease causing severe acute respiratory syndrome and diverse injuries in other systems [31-34]. SA and CH are believed to possess potential as neurodrugs for AD due to their ability to inhibit several neuropathologically-relevant enzymes [35]. However, clues of neuroprotective properties were found experimentally only for CH which inhibited *in vitro* amyloid aggregation [36], whereas the same inhibitory activity, predicted *in silico* for SA by some of us [37], had not been validated before on an experimental basis.

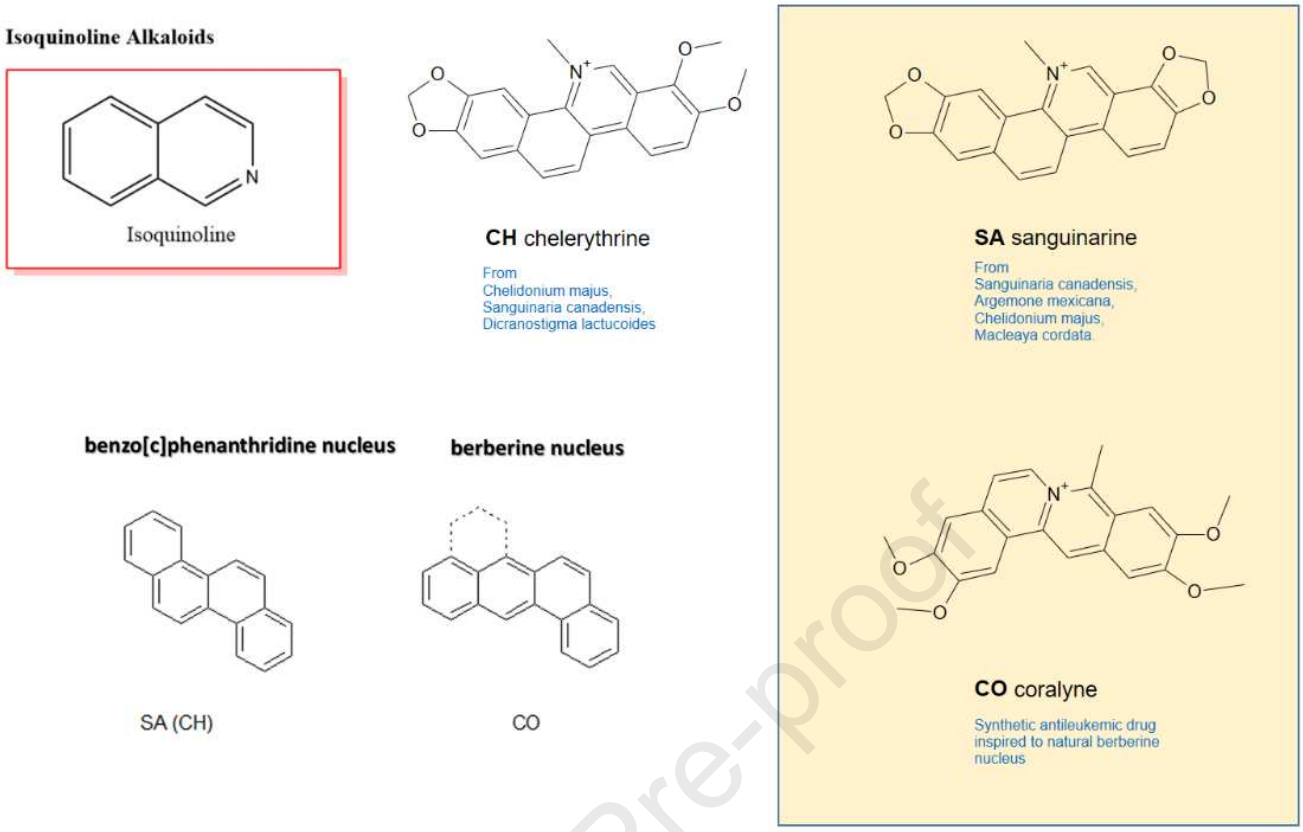


93

94 **Fig. 1.** The isoquinoline alkaloids of synthetic (CO) and plant **(**CH and SA) origin investigated in
95 this work. All share an isoquinoline core (up, left) but are based on two different polycycle
96 rearrangements (bottom, left).

97

98 The scope of this work was to investigate the interaction between tetracyclic aromatic structures
99 endowed with benzo[*c*]phenanthridine (SA, CH) and berberine nuclei, respectively (CO, Figure 1)
100 with $A\beta_{1-42}$ peptide, by means of ThT fluorescence and CD spectroscopies to evaluate their effects
101 on the aggregation of $A\beta_{1-42,}$ and by SPR assays to evaluate the entity of these interactions.

102 Experimental data were further corroborated by *in silico* studies, through molecular docking
103 simulations, to unveil preferential binding modes of ligands to different aggregated forms of $A\beta_{1-42}$,
104 and by molecular dynamics simulations to deepen the effects of these compounds in early
105 aggregation stages of $A\beta_{1-42}$.

106

## 2. Materials and Methods

**2.1 Chemicals** $A\beta_{1-42}$ peptide (for CD and SPR), SA, CH, SA isoquinoline alkaloids andall other chemicals and solvents were purchased from Sigma-Aldrich (Amsterdam, The Netherlands). $A\beta_{1-42}$ peptide for ThT assay was purchased from rPeptide (GA, USA).

### 2.2 $A\beta_{1-42}$ peptide solubilization

Solutions of recombinant $A\beta_{1-42}$ peptide were prepared according to a previously published procedure [38]. In short, $A\beta_{1-42}$ was sequentially dissolved in hexafluoroisopropanol (HFIP) and DMSO. The DMSO was removed from the $A\beta_{1-42}$ solution by using a HiTrap™ desalting column (GE Healthcare, Zwijndrecht, The Netherlands) and elution with PBS at pH 7.4. We measured the $A\beta_{1-42}$concentration by the Coomassie (Bradford, UK) Protein Assay Kit (ThermoFisher, Landsmeer, The Netherlands) and, afterwards, the final concentration required for the subsequent experiments was achieved by dilution. Aβ peptide aggregation, in the presence or absence of SA, CH and CO, was evaluated at 37°C under quiescent conditions.

### 2.3 Thioflavin-T assay

Amyloid aggregation was measured by a ThT fluorescence assay. The $A\beta_{1-42}$ concentration was adjusted to 25 μM using PBS buffer (pH 7.4), while a final ThT concentration of 12 μM was realized in a 96-well plate (Greiner flat bottom transparent black, Sigma–cat. M9685). Fluorescence intensity was measured at 37°C using an automated well-plate reader (Tecan Infinite 200 PRO) at an excitation wavelength of 450 nm and emission detection from 480 to 600 nm. The fluorescence intensity from ThT at its maximum value (485 nm) was reported in a graph for the three complexes with the ligands (C=25 μM). Measurements were performed in triplicate, averaged the values recorded and subtracted background measurements that corresponded to buffer containing 12 μM ThT and the tested isoquinoline alkaloids. Measurements were performed after incubation for2 h to allow Aβ to aggregate.

## 2.4 CD and UV experiments

The CD experiments were conducted as previously described [39-49]. The spectra were obtained using a JascoJ-715 spectropolarimeter coupled to a PTC-348WI temperature control system, and a quartz cell with a path length of 1 cm, at 37°C with a response of 1 s, a scanning speed of 100 nm/min and a 2.0 nm bandwidth. All the spectra were averaged over three scans. Experiments were carried out using a 5 μM concentration of $A\beta_{1-42}$ in PBS (overall volume = 2 ml, pH 7.2) and a twofold concentration of ligands. Spectra were collected after incubation at 37°C for 0.5, 24 and 48 h.

## 2.5 Surface plasmon resonance (SPR) experiments

Surface plasmon resonance (SPR) binding assays were performed on a Biacore 3000 (GE Healthcare). $A\beta_{1-42}$ peptide was immobilized on a CM5 chip through an amine coupling procedure at 100 μg/mL in 10 mM sodium acetate (pH 4) at 2 μL/min until reaching an immobilization level of ~400 RU. Binding assays were carried out by injecting 90 μL of analyte, at 20 $\mu L\, min^{-1}$. Experiments were carried out using PBS as running buffer. The association phase ($k_{on}$) was followed for 270 s, whereas the dissociation phase ($k_{off}$) was followed for 300 s. The reference chip sensorgrams were subtracted to sample sensorgrams. After each cycle, the sensor chip surface was regenerated with a 10mM NaOH solution for 30 s. Analyte concentrations were for cheletrine 20, 40, 80 and 100 μM, sanguinarine 100, 300, 500, 700, 900 and 1100 μM and for coralyne 5, 20, 30, 40, 50, 70 μM. Experiments were carried out in duplicates. Kinetic parameters were estimated assuming a 1:1 binding model and using version 4.1 Evaluation Software (GE Healthcare).

## *2.6 In silico* studies

In all computational studies, as initial $A\beta_{1-42}$ conformations we utilized S-shape and U-shape fibril models (PDB codes: 2LMN and 2MXU) and three of the most representative monomeric models from previous extensive computational studies[50].

## 2.7 Ligand parameterization

Fully-protonated structures of the three compounds (CO, SA, CH) were optimized by gaussian 09 software[51], utilizing Hartree-Fock method and 6-31G* basis set. AM1-BCC method[52] implemented in the AmberTools 19 package was used to derive charges of all atoms. Parameters for bonds, valence and dihedral angles were adapted from General Amber Force Field[53] based on structural similarity.

## 2.8 Docking

Global molecular docking of compounds to the monomeric and fibrillar structures of $A\beta_{1-42}$ was performed using AutoDock 4.2.6 software[54] allowing flexibility of the ligand with rigid conformation of the receptor due to computational limitations. The algorithm was set to generate 100 initial docking positions and subsequently perform clustering using 10, 15, and 15Å criteria for monomeric, tetrameric, and fibril structures, respectively, to obtain most probable docking positions (modes) of the compounds. Two different cutoff values were used due to large size differences between monomeric and other systems. AutoDock 4.2 was selected for docking, because it was found to provide more reliable binding energies than AutoDock Vina in the recent studies[55].

## 2.9 Molecular dynamics simulations

Two series of molecular dynamics (MD) simulations were performed: (i) fibrillar structures with the compounds bound to them, obtained through docking procedure, and (ii) 16 non-bound semi-extended $A\beta_{1-42}$ chains in the presence and absence of compounds. MD simulations of fibrillar $A\beta_{1-42}$ with compounds were performed using Amber ff14sb [56] force field with TIP3P water model[57], which should provide reliable results for these systems. Due to computational restrictions, MD simulations were performed for top 2 binding modes of each system, each of 10 separate trajectories, reaching in total 1 µs for each of the binding modes.

For MD simulations of 16 chains, we used an in-house algorithm to put pre-generated semi-extended $A\beta_{1-42}$ chains of random conformations as close to each other as possible, with the

restriction to keep minimum distance of 8Å between any heavy atoms of different chains to avoid possible bias coming from initial orientation of the chains. Such system was hydrated by adding approximately 47500 water molecules and charge was neutralized by inserting counterions, resulting in truncated octahedron boxes of total volume of approximately 1549 nm[52]. In simulations with compounds, small molecules were placed between $A\beta_{1-42}$ chains using the same criterion. In all simulations, initial orientations of $A\beta_{1-42}$ chains and compounds were identical.

Obtained systems were energy minimized, using steepest descent and conjugate gradient algorithm and equilibrated for 1ns. For each type of system, two trajectories were run, each of 800ns and then recorded 40,000 snapshots from second halves (400-800ns) were analyzed. To better capture aggregation effects in simulations of systems containing 16 chains, we utilized state-of-the-art Amber ff19sb force field[58] coupled with OPC water model[59], which should provide reliable results, especially for binding-dissociation process. Analysis of these simulations included root-mean-square deviation (RMDd) using initial structure as a reference, radius of gyration (Rg), solvent-accessible surface area (SASA) using LCPO method[60] and secondary structure determinations with DSSP[61] algorithm implemented into Amber19 package and various distance calculations. Distance criterion of 6.5 Å between centers of mass of two side-chains is used to determine a contact between chains, and a criterion of 5 contacts was used to determine the size of the oligomer (e.g. two chains have to form at least 5 contacts to be named as dimer), as in our previous work[62] to discard structures forming weak interaction due to accidental proximity of the chains.

### 2.10 Molecular Mechanics - Poisson Boltzmann Surface Area (MM/PBSA) method

MM-PBSA is a post-processing method which was used to calculate the free energy difference, $\Delta G_{bind}$, between the free and bound states of a molecule complex: receptor and ligand. $\Delta G_{bind}$ is calculated for a set of selective snapshots from simulation trajectory and is defined as follows:

$$\Delta G_{bind} = \Delta E_{elec} + \Delta E_{vdW} + \Delta E_{SUR} + \Delta E_{PB} - T\Delta S, (1)$$

where $\Delta E_{elec}$ and $\Delta E_{vdW}$ are differences in electrostatic and van der Waals energy components, respectively, $\Delta E_{SUR}$ and $\Delta E_{PB}$ describe differences in non-polar and polar solvation free energies, respectively, and $T\Delta S$ represents the entropic contribution.

In this study, MM/PBSA methods implemented into the AmberTools 19 package was used to estimate $\Delta G_{bind}$ of compounds to fibrillar models using second halves of performed MD simulations. As a standard procedure, for energy calculation in MM/PBSA procedure we used the same force field adopted to perform the simulations, however, without cutoff for electrostatic and van der Waals interactions. The entropic term, $T\Delta S$, was estimated by normal mode approximation method, where $\Delta E_{PB}$ was obtained by solving numerically linearized Poisson-Boltzmann equation and $\Delta E_{SUR}$ was calculated from the following equation:

$$\Delta E_{SUR} = \alpha \times SASA + \beta, (2)$$

where SASA was calculated using LCPO method[60], regression coefficient $\alpha$ was set to 0.005 and the regression offset $\beta$ was set to 0.

## 3. Results and Discussion

### 3.1 Modulation of $A\beta_{1-42}$ aggregation

To obtain preliminary insights into the ability of isoquinoline alkaloids to modulate amyloid $A\beta_{1-42}$ aggregation we evaluated thioflavin (ThT) fluorescence intensity after incubation [63]. The $A\beta_{1-42}$ monomer (25 μM) was incubated with SA, CH or CO (25 μM) at 37°C for 2 h which is considered a sufficient time for accumulation of oligomeric Aβ species [64]. The extent of aggregation of $A\beta_{1-}$

$_{42}$ within this incubation time was assessed by recording the fluorescence emission of ThT (12 μM, $\lambda_{ex}$ = 450 nm, $\lambda_{em}$ = 485 nm) (Figure 2).

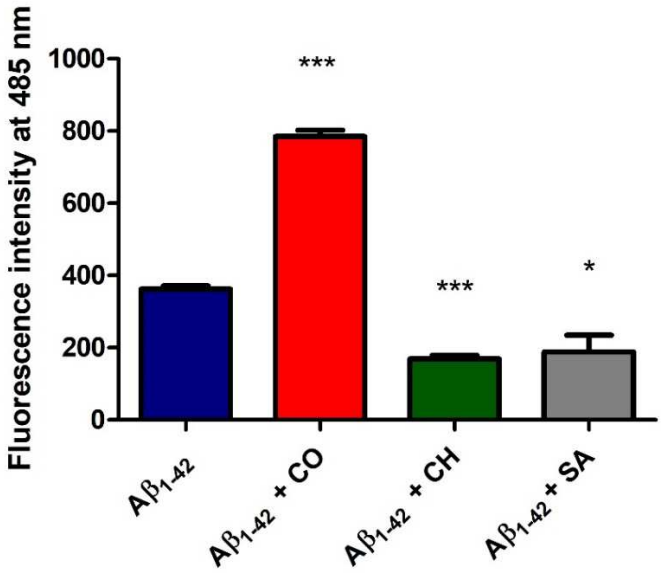


**Fig. 2. SA and CH inhibit ThT-positive amyloid fibril formation of Aβ$_{1-42}$, whereas CO induces ThT-positive amyloid fibril formation.** Solutions containing Aβ$_{1-42}$ at a concentration of 25 μM were incubated in the presence and absence of **SA, CH and CO (at 1:1 ratio)** at 37°C for 2 h. Amyloid fibril formation was detected using ThT fluorescence intensity measurements at a fluorescence emission wavelength of 485 nm upon excitation at 450 nm. The reported values represent the results obtained from three independent experiments. The statistical significance of the replicates was assessed by p-values using paired two-tailed t-tests (GraphPad Prism).

*p < 0.05, **p < 0.01, and ***p < 0.001 compared with the control ('Aβ$_{1-42}$').

Data show that SA and CH reduce the ThT fluorescence signal by ~40% compared with Aβ$_{1-42}$ in the absence of these compounds. On the other hand, the berberine-like CO increased the aggregation level of Aβ$_{1-42}$ as indicated by a strong two-fold increase in ThT fluorescence intensity compared to untreated Aβ$_{1-42}$. These results clearly show that berberine-like and benzo[*c*]phenanthridine alkaloids modulate differently Aβ$_{1-42}$ aggregation.

### 3.2 $A\beta_{1-42}$ conformational response to isoquinoline alkaloids

To investigate if the observed effects of isoquinoline alkaloids on $A\beta_{1-42}$ aggregation were accompanied by conformational variations, we performed circular dichroism (CD) time-dependent studies. The aggregation of $A\beta_{1-42}$, which reportedly coincides with increasing β-sheet content [65], was monitored using CD at different time points of incubation (0.5, 24 and 48 h, in PBS at 37°C; Figure 3). The obtained time-dependent CD profiles of $A\beta_{1-42}$ showed spectral changes in agreement with those reported in literature [11, 66] with a progressive transition towards a β-sheet conformation at 24 h indicated by a broad band centered at ~225 nm, that is a spectral element previously assigned to this secondary structure in many amyloid systems [67-72].

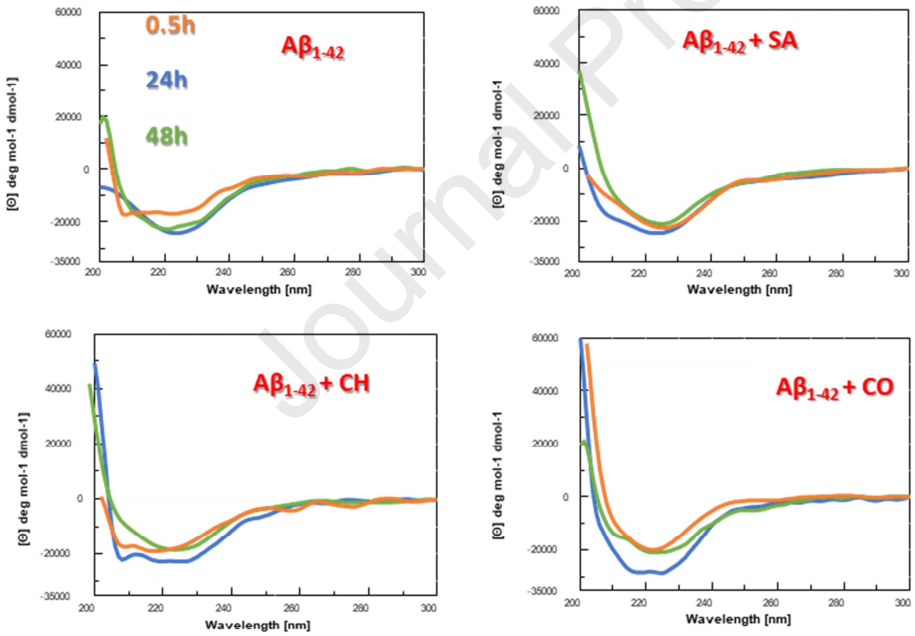


**Fig. 3. Conformational response of $A\beta_{1-42}$ peptide to SA, CH and CO.** Circular dichroism spectra of $A\beta_{1-42}$ (5 μM concentration in PBS, black line) and $A\beta_{1-42}$ in the presence of isoquinoline alkaloids (1:2 molar ratio, peptide: small molecule) after 0.5 (orange), 24 (blue), and 48 (green) h of incubation at 37°C.

This progression was also confirmed by deconvolution percentages reported in table S1. At longer incubation times molar ellipticity intensity at 225 nm showed a tendency to decrease (Figure 3) suggestive of amyloid aggregation/precipitation as previously observed under similar conditions [66]. In parallel, $A\beta_{1-42}$ was incubated, under the same experimental conditions, with the isoquinoline alkaloids (which did not contribute to the observed CD signal).

Remarkably, the presence of CO, already at t=0.5 h of analysis, (Figure 3) favors a β-like structure as indicated by a minimum at ~225 nm, together with the secondary structures content reported in table S1, that, in the following 24 h, slightly shifts toward higher wavelengths (Figure 3). The observed increase of Cotton effect for $A\beta_{1-42}$ in the presence of CO at 24 h (Figure 3) can be ascribed to a stabilization of these secondary structures [73-78]. When comparing the CD spectra of $A\beta_{1-42}$ in the presence of all three compounds after 24 h, it became apparent that the presence of the three isoquinoline alkaloids induced differences in the structural organization of $A\beta_{1-42}$ (Figure 3). The observed changes, impacting on both intensity and shape of spectra, were already described by Guo et al. [69], suggesting that benzo[*c*]phenanthridines partly limited β-sheet content of $A\beta_{1-42}$ leading to new structural elements. The effects is more appreciable for CH while the main significant variations are evident in the 210-220 nm range for SA.

### 3.3 Isoquinoline alkaloids interact with $A\beta_{1-42}$

To further evaluate the ability of isoquinoline alkaloids to interact with $A\beta_{1-42}$ we carried out SPR assays [79]. Binding profiles for all three molecules (Figure 4) suggested the formation of complexes, in a concentration-dependent manner. Freshly dissolved $A\beta_{1-42,}$ after HFIP treatment, was covalently immobilized on Sensor chip [80] . Kinetic parameters, reported in Table 1, allowed the estimation of thermodynamic dissociation constant values that appear in the low, for CO, high, for SA, and very high, for CH, micromolar range. The higher affinity exhibited by CO compared to CH and SA can be due to the faster association phase. Our data are in agreement with a previous study [80] that showed the ability of berberine-like inhibitors of $A\beta_{1-42}$ to interact with the polypeptide at low micromolar $K_D$ values [80].

**Table 1.** SPR based equilibrium dissociation constants ($K_D$) and kinetic parameters for the interaction of $A\beta_{1-42}$ with SA, CH and CO using the BIA evaluation v.4.1 software. Data reported were obtained through SPR analyses using small molecules as analyte on immobilized $A\beta_{1-42}$.

| | $k_{on}$ ($M^{-1}s^{-1}$ x $10^4$) | $k_{off}$ ($s^{-1}$ x$10^{-3}$) | $K_D$ (µM) |
|---|---|---|---|
| **Sanguinarine (SA)** | 13.1 | 6.07 | 463 |
| **Cheletrine (CH)** | 5.14 | 19.7 | 3.83*10 $^3$ |
| **Coralyne (CO)** | 983 | 11.4 | 11.6 |

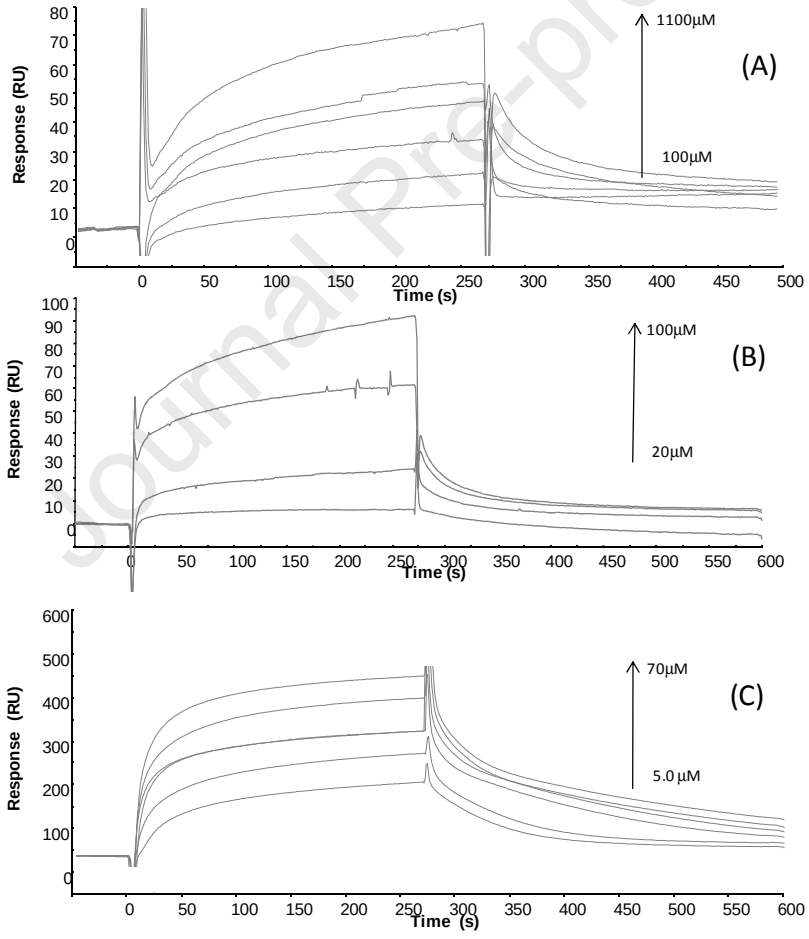


**Fig. 4.** Overlay of sensorgrams for the binding to immobilized $A\beta_{1-42}$ of (**A**) SA, (**B**) CH and (**C**) CO.

### 3.4 Computational study of the interaction of SA, CH and CO with monomeric and fibrillar $A\beta_{1-42}$

To deepen the molecular-level interactions responsible of modulating effects of aggregative mechanism of $A\beta_{1-42}$ displayed by small molecules we performed *in silico* studies.

### 3.5 Binding energies

#### *3.5.1 Docking of ligands to monomers*

The binding energies of the three ligands were estimated by means of Molecular Docking. Since Aβ peptides are intrinsically disordered, their native structures are transient and cannot be resolved experimentally.

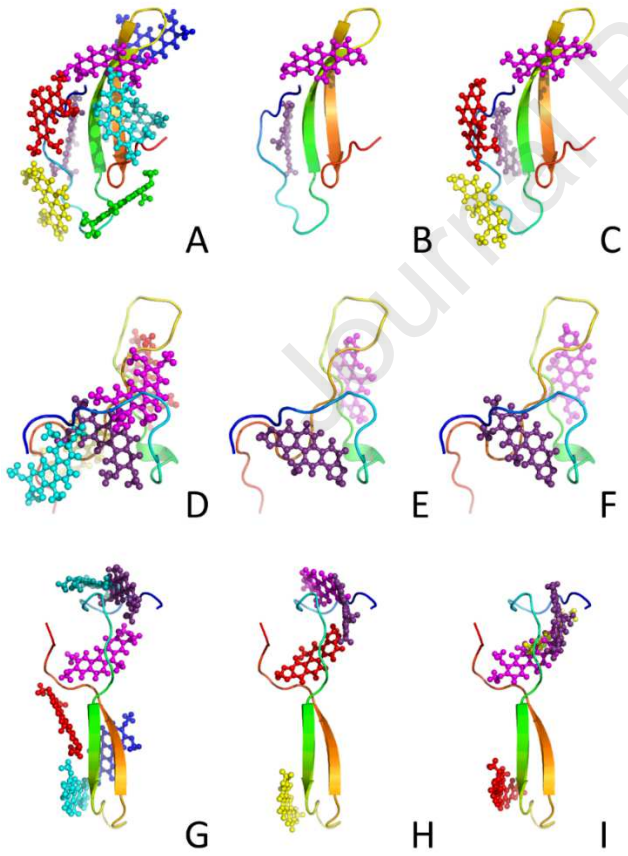


**Fig. 5.** Representations of docking positions of CO (left column: A, D, G), SA (middle column: B, E, H), and CH (right column: C, F, I) to three models of monomeric $A\beta_{1-42}$ (presented as rainbow-colored cartoons).

Therefore, for our simulations we adopted three most representative $A\beta_{1-42}$ monomeric models obtained by clustering ensembles of monomeric $A\beta_{1-42}$ conformations at 300K from extensive all-atom Replica-Exchange and conventional MD simulations with explicit water model performed with various Amber and CHARMM force fields, [50] as targets (Figure 5). As expected for similar small compounds, their modes of interactions appeared quite similar, but significant differences were observed in the number of possible binding modes (Table 2), which is higher for CO for all three monomeric structures. Conversely, the lowest number of binding modes was found for SA suggesting a more selective binding mechanism toward $A\beta_{1-42}$ structure with respect to the other compounds. The drug-amyloid interactions are stabilized by both hydrophobic and hydrogen bonds (three for SA and CH and one for CO, Figure 6). Interestingly, CH and SA, contrary to CO, form hydrogen bonds with two histidine residue (His13 and His14), that are reported as responsible of the binding of ions, e.g. $Cu^{2+}$, which impacts $A\beta_{1-42}$ aggregation [81].

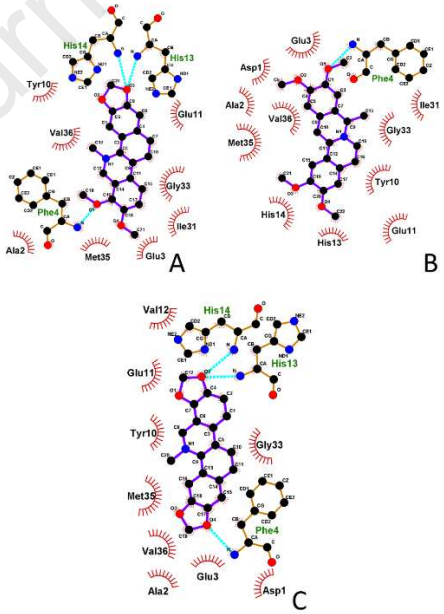


**Fig. 6.** Schematic representation of the strongest binding mode of monomeric $A\beta_{1-42}$ to compounds (monomeric model 2, binding mode 1; see Table 2 for more details) showed in 2D form for: A) CH, B) CO, C) SA. $A\beta_{1-42}$ residues involved in hydrophobic interactions with compounds are showed by

red lines and black three-letter residue codes, hydrogen bonds are represented by cyan dashed lines and green three-letter residue codes. For clarity, hydrogens are not presented on the plot.

Averaging over representative $A\beta_{1-42}$ models, in the best docking modes (mode 1 with the strongest binding in Table 2) obtained binding energies indicate that all compounds strongly bind to monomeric $A\beta_{1-42}$. The highest interaction energy was observed for the least structured model 2, due to the disordered and extended character of this conformation allowing compounds to maximize number of hydrogen bonds between molecules maintaining high number of hydrophobic contacts (Table 3).

**Table 2.** AutoDock-predicted binding energies (kcal/mol) for the binding of the compounds CO, SA, and CH to three representative amyloid monomeric models obtained in the previous simulation study[50]

| | $A\beta_{1-42}$ **Model 1** | | | $A\beta_{1-42}$ **Model 2** | | | $A\beta_{1-42}$ **Model 3** | | |
|---|---|---|---|---|---|---|---|---|---|
| **Binding Mode** | **CO** | **SA** | **CH** | **CO** | **SA** | **CH** | **CO** | **SA** | **CH** |
| 1 | -8.03 | -9.10 | -8.59 | -10.17 | -10.26 | -10.07 | -9.44 | -9.07 | -8.82 |
| 2 | -6.68 | -7.24 | -7.39 | -7.53 | -8.58 | -8.36 | -8.11 | -8.99 | -8.31 |
| 3 | -6.36 | | -6.05 | -7.52 | | | -6.68 | -8.69 | -7.05 |
| 4 | -6.24 | | -6.03 | -7.07 | | | -6.58 | -6.87 | -6.86 |
| 5 | -5.57 | | | -7.00 | | | -5.84 | | |
| 6 | -5.42 | | | | | | -5.30 | | |
| 7 | -5.34 | | | | | | | | |
| 8 | -5.28 | | | | | | | | |

**Table 3.** Number of hydrogen bonds (HB) and hydrophobic interactions (HI) between monomeric $A\beta_{1-42}$ models and the ligands CO, SA, and CH in the strongest binding mode (mode 1).

| | $A\beta_{1-42}$ **Model 1** | | $A\beta_{1-42}$ **Model 2** | | $A\beta_{1-42}$ **Model 3** | |
|---|---|---|---|---|---|---|
| | *HI* | *HB* | *HI* | *HB* | *HI* | *HB* |
| *CO* | *10* | *1* | *11* | *1* | *9* | *1* |
| *SA* | *10* | *1* | *9* | *3* | *7* | *1* |
| *CH* | *9* | *1* | *8* | *3* | *7* | *1* |

### *3.5.2 Docking of ligands to $A\beta_{1-42}$ tetramers*

As oligomeric states are a bridging step between monomers and fibrils, we decided to study the impact of the three ligands on tetramers, that are considered crucial in $A\beta_{1-42}$ aggregation[82], by using models obtained in previous multi-scale MD simulations [62]. Similar to the monomeric $A\beta_{1-42}$, SA exhibited minor binding modes for all three tetrameric models (Table 4 and Figure S1) confirming major selectivity of interaction. Average binding energies for first binding indicate a slight major value for SA and CH with respect to CO: the small differences in binding of compounds to monomeric and tetrameric forms are probably due to compact forms of $A\beta_{1-42}$ tetramers, which did not allow many interactions with drugs even when more chains and possible binding sites are available. In both 2LMN and 2MXU models, the three ligands can bind in different regions depending on the docking mode (Figures S2 and S3 in Supporting Information). In the docking mode with the lowest energy, they are all preferentially located in the loop region of 2LMN, while for 2MXU CO and CH seem to prefer the terminal part, while SA is mainly located in the middle of the structure. In analogy to the monomeric case, SA is endowed with the poorest variety in docking positions compared to the other two ligands (Figures S2 and S3, and Table 5).

**Table 4.** AutoDock-predicted binding energies (kcal/mol) for the binding of the CO, SA, and CH to three representative amyloid tetrameric models obtained in the previous simulation study [62] (models 1, 2, and 3 correspond to tetramers 1, 3, and 5 from the mentioned work, respectively).

| | $A\beta_{1-42}$ **tetramer 1** | | | $A\beta_{1-42}$ **tetramer 2** | | | $A\beta_{1-42}$ **tetramer 3** | | |
|---|---|---|---|---|---|---|---|---|---|
| **Binding Mode** | **CO** | **SA** | **CH** | **CO** | **SA** | **CH** | **CO** | **SA** | **CH** |
| 1 | -9.06 | -9.97 | -9.72 | -9.36 | -9.52 | -9.26 | -8.21 | -10.45 | -9.81 |
| 2 | -8.48 | -9.89 | -8.93 | -8.84 | -9.46 | -9.05 | -7.94 | -8.44 | -8.43 |
| 3 | -7.56 | -9.14 | -8.78 | -8.80 | -9.13 | -7.91 | -7.24 | -8.26 | -8.32 |
| 4 | -7.51 | | -7.19 | -7.28 | -8.34 | -7.42 | -7.02 | -7.96 | -7.57 |
| 5 | -6.43 | | -7.13 | -7.25 | -7.52 | -7.33 | -7.00 | -7.68 | -7.50 |
| 6 | -5.77 | | -6.55 | -7.04 | | -6.96 | -6.80 | | -6.88 |
| 7 | | | | | | | -6.55 | | -6.50 |
| 8 | | | | | | | -6.01 | | -6.48 |

Assuming that protofibrils and fibrils have similar structures [83], we used the fibrillar structures 2LMN and 2MXU deposited in PDB databank, for further docking simulation.

With binding energies ranging from -10.4 to -12.2 kcal/mol (Table 5), all ligands are tightly associated with protofibril models. The identified potential for the ligands to interact with both monomeric and protofibrillar $A\beta_{1-42}$ suggests ample means for the ligands to modulate the subsequent aggregation process.

Molecular Mechanics - Poisson Boltzmann Surface Area (MM-PBSA) docking assays on two compounds provided similar results (Figures S4, S5 and Table S2).

**Table 5.** AutoDock-predicted binding energies (kcal/mol) of the clustered orientations with 2LMN and 2MXU fibril models.

| | 2LMN | | | 2MXU | | | |
|---|---|---|---|---|---|---|---|
| **Mode** | **CO** | **SA** | **CH** | **CO** | **SA** | **CH** | **Color** |
| 1 | -12.12 | -12.16 | -10.93 | -10.41 | -11.76 | -10.89 | Purple |
| 2 | -11.90 | -10.71 | -10.83 | -9.70 | -10.92 | -10.36 | Magenta |
| 3 | -10.07 | -10.50 | -9.83 | -8.71 | -10.09 | -9.73 | Red |
| 4 | -10.00 | -10.37 | -9.71 | -7.14 | -9.98 | -7.96 | Yellow |
| 5 | -9.97 | -9.94 | -9.60 | -6.34 | | -7.87 | Cyan |
| 6 | -8.84 | | -9.56 | | | -7.80 | Teal |
| 7 | -8.78 | | -9.42 | | | | Blue |
| 8 | -8.37 | | -8.15 | | | | Green |
| 9 | -6.72 | | -6.95 | | | | Darkgrey |
| 10 | -6.21 | | | | | | Lightgrey |

### 3.5.3 Molecular Dynamic Simulations

I*n silico* prediction of binding of the alkaloids to $A\beta_{1-42}$ provided limited information on the effect of complex formation on the rate of $A\beta_{1-42}$ aggregation. Thus, we performed MD simulations with 16 $A\beta_{1-42}$ chains in the absence or presence of CO and SA to mimic the first stages of $A\beta_{1-42}$ aggregation from semi-extended non-interacting chains. The simulation started from the initial configuration of the 16 non-interacting randomly generated $A\beta_{1-42}$ chains in the presence of ligands in a 1:1 ratio (Figure 7). For each set, we carried out two trajectories of 800 ns: this short interval even if does not allow reaching equilibrium provides insights the initial steps of the aggregation.

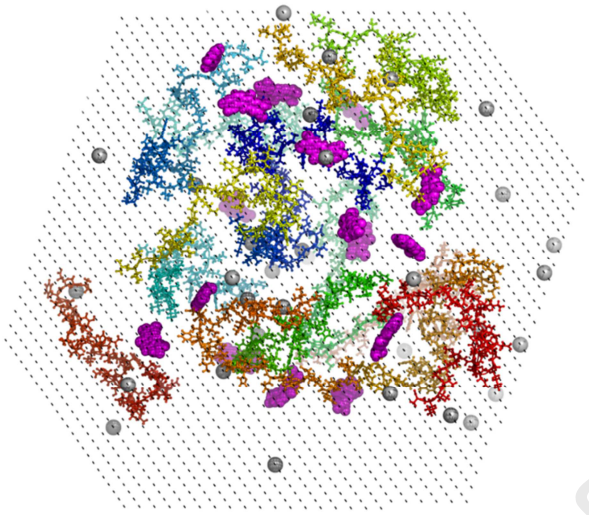

386 .

387 **Fig. 7.** Initial structure of the 16 $A\beta_{1-42}$ chains with SA in 1:1 ratio. $A\beta_{1-42}$ is represented by ball-
388 and-sticks, SA by magenta spheres, counter ions by light-grey sphere, water by black dots.

389 Simulations showed that the flexibility of the chains was unaffected by the presence of the ligands
390 (Table 6), as RMSD, gyration radius Rg, solvent accessible surface area (SASA), and end-to-end
391 (N-C) distance did not vary significantly in absence or presence of the ligand. This was expected
392 due to the semi-extended nature of the initial $A\beta_{1-42}$ chains, which in the early aggregation steps
393 firstly try to hide hydrophobic residues from the solvent and only then form stable interactions with
394 other chains forming oligomeric structures. [84, 85]. In general, calculated properties are quite
395 dispersed, which is visible as high standard deviation values in Table 6, a feature caused by
396 averaging over 16 chains, 2 trajectories and snapshots from the second halves of the simulations
397 which are not fully equilibrated, and by the fact that $A\beta_{1-42}$ chains are subjected to large
398 conformational changes. However, even relatively small changes at early aggregation steps caused
399 e.g. by the presence of external compounds, can significantly impact aggregation pathways and
400 fibrilization process [86, 87]. It was also previously reported that the beta content of $A\beta_{1-42}$
401 monomers exponentially affects the aggregation rate [88]. The most notable differences were found
402 in the amyloid secondary structure content: SA, unlike CO, increased α-helical content in $A\beta_{1-42}$
403 chains, and destabilized β-strands (much larger variation with SA on Figure S6 and Table 6). This
404 finding suggests that SA slowed fibril formation process, while CO enhances formation of fibril-

like structures, and is consistent with our experimental results. Destabilization of the β-structures of the $A\beta_{1-42}$ due to the presence of the ligand is known to modulate nucleation and slow down the aggregation process [89]. Furthermore, the MD simulations indicated a decrease in contacts between chains, confirming that compounds are able to directly interact with the single $A\beta_{1-42}$ chains, to alter the equilibrium between monomeric and oligomeric forms (Figure S7).

**Table 6.** Calculated average properties of the $A\beta_{1-42}$chains from simulations of 16 chains with standard deviations.

| | $A\beta_{1-42}$ | $A\beta_{1-42}$+ CO | $A\beta_{1-42}$+ SA |
|---|---|---|---|
| RMSD [Å] | 11.15 ± 0.50 | 11.27 ± 0.36 | 11.52 ± 0.37 |
| Rg [Å] | 14.16 ± 0.34 | 14.75 ± 0.69 | 14.17 ± 0.36 |
| SASA [$nm^2$] | 562.8 ± 28.3 | 573.8 ± 22.0 | 560.5 ± 21.3 |
| N-C distance [Å] | 33.00 ± 2.13 | 33.87 ± 3.02 | 33.37 ± 1.91 |
| Number of contacts between chains | 2.44 ± 5.71 | 1.88 ± 4.07 | 1.95 ± 4.54 |
| Alpha content [%] | 3.23 ± 1.21 | 3.23 ± 1.28 | 4.40 ± 0.85 |
| Beta content [%] | 3.85 ± 0.74 | 4.55 ± 0.74 | 3.85 ± 1.73 |

Both ligands reduced the population of monomers: a remarkable variation in the population of tetramers, heptamers, 14- and 15-mers (Figure S7) was observed, which means that aggregation pathways to the fibril state are deeply modified by the ligands. In addition to size of the oligomers, secondary content is the prevalent factor governing aggregation rate of $A\beta_{1-42}$ [90], explaining opposite effects of the SA and CO on the aggregation.

## 4. Conclusion

In this work, we demonstrated that aromatic tetracycles with benzo[*c*]phenanthridine and berberine nuclei and similar functionalization of the aromatic core may oppositely affect the aggregation of

422 $A\beta_{1-42}$ peptide. While benzo[*c*]phenanthridines SA and CH significantly inhibited aggregation, the
423 berberine-like CO increased propensity for $A\beta_{1-42}$ to aggregate, showing also the highest affinity for
424 monomeric $A\beta_{1-42}$, as revealed by SPR experiments, and displayed the highest variety of binding
425 modes (as found *in silico*). These observations suggest that, different from benzo[*c*]phenanthridines,
426 the bent berberine-like structure of CO can be accommodated in a higher number of diverse $A\beta_{1-42}$
427 conformations. The presence of CO also led to increased $A\beta_{1-42}$ β-content as revealed by CD
428 experiments and MD calculations: this effect appears in perfect agreement with the promotion of
429 $A\beta_{1-42}$ aggregation observed in the ThT assay. Both docking and MM-PBSA simulations showed
430 that all three studied alkaloids interact with monomeric, oligomeric and protofibrillar $A\beta_{1-42}$. Our *in*
431 *silico* study revealed that SA inhibits the assembly of $A\beta_{1-42}$ into aggregates as a result of helix
432 stabilization in the $A\beta_{1-42}$ amyloid structure. On the contrary, the aggregation promoting effect
433 caused by CO possibly occurs through enhancement of the β structures, which are predominantly
434 reported in the fibril state. Interestingly, both benzo[*c*]phenanthridine and berberine derivatives are
435 able to modulate the amyloid aggregation pathways by showing differences in the population of
436 different oligomeric states, and in particular the $A\beta_{1-42}$ oligomer assembly state undergoes
437 noteworthy changes upon ligand binding.

438 Finally, since berberine and Ber-D (Figure S7), compounds differing from CO by carrying one non-
439 aromatic ring (berberine) or free hydroxyl-groups besides the non-aromatic ring (Ber-D), both
440 inhibit $A\beta_{1-42}$ aggregation [22], future synthetic efforts and, biological studies should be carried out
441 on chelerythrine-derived compounds CH-D1 and CH-D2 (Figure S8) as promising candidates as
442 neurodrugs in the family of the benzo[*c*]phenanthridine alkaloids[22].

443

444 **Funding**

445 We are grateful to the financial support received from Campania Region, Italy [POR-FESR 2014-
446 2020 project PON03PE_0060_4], ”Combattere la resistenza tumorale: piattaforma integrata

multidisciplinare per un approccio tecnologico innovativo alle oncoterapie-Campania Oncoterapie" (Project N. B61G18000470007) and ZonMw for Memorabel project "Exploring the potential of multi-target treatment for Alzheimer's disease" (Project N. 733050304). Mai Suan Li was supported by Department of Science and Technology, Ho Chi Minh city, Vietnam (grant No. 07/2019/HĐ-KHCNTT).

## Conflict of interest

The authors declare that there is no conflict of interest regarding the publication of this article.

## Supplementary data

Supplementary data, including CD deconvolution, computational docking and MD data were provided.

## References

[1] J.-C. Rochet, P.T. Lansbury, Amyloid fibrillogenesis: themes and variations, Current Opinion in Structural Biology, 10 (2000) 60-68.
[2] J. Nasica-Labouze, P.H. Nguyen, F. Sterpone, O. Berthoumieu, N.-V. Buchete, S. Coté, A. De Simone, A.J. Doig, P. Faller, A. Garcia, A. Laio, M.S. Li, S. Melchionna, N. Mousseau, Y. Mu, A. Paravastu, S. Pasquali, D.J. Rosenman, B. Strodel, B. Tarus, J.H. Viles, T. Zhang, C. Wang, P. Derreumaux, Amyloid β Protein and Alzheimer's Disease: When Computer Simulations Complement Experimental Studies, Chemical Reviews, 115 (2015) 3518-3563.
[3] J. Weller, A. Budson, Current understanding of Alzheimer's disease diagnosis and treatment, F1000Research, 7 (2018) 1161.
[4] K. Blennow, M.J. de Leon, H. Zetterberg, Alzheimer's disease, The Lancet, 368 (2006) 387-403.
[5] L. Gu, Z. Guo, Alzheimer's Aβ42 and Aβ40 peptides form interlaced amyloid fibrils, Journal of Neurochemistry, 126 (2013) 305-311.
[6] Z. van Helmond, J.S. Miners, P.G. Kehoe, S. Love, Oligomeric Aβ in Alzheimer's Disease: Relationship to Plaque and Tangle Pathology,APOEGenotype and Cerebral Amyloid Angiopathy, Brain Pathology, 20 (2010) 468-480.

[7] A. Jan, O. Adolfsson, I. Allaman, A.-L. Buccarello, P.J. Magistretti, A. Pfeifer, A. Muhs, H.A. Lashuel, Aβ42 Neurotoxicity Is Mediated by Ongoing Nucleated Polymerization Process Rather than by Discrete Aβ42 Species, Journal of Biological Chemistry, 286 (2011) 8585-8596.
[8] K.H. Gylys, J.A. Fein, F. Yang, C.A. Miller, G.M. Cole, Increased cholesterol in Aβ-positive nerve terminals from Alzheimer's disease cortex, Neurobiology of Aging, 28 (2007) 8-17.
[9] A.J. Doig, P. Derreumaux, Inhibition of protein aggregation and amyloid formation by small molecules, Current Opinion in Structural Biology, 30 (2015) 50-56.
[10] F. Re, C. Airoldi, C. Zona, M. Masserini, B.L. Ferla, N. Quattrocchi, F. Nicotra, Beta Amyloid Aggregation Inhibitors: Small Molecules as Candidate Drugs for Therapy of Alzheimers Disease, Current medicinal chemistry, 17 (2010) 2990-3006.
[11] C. Vicidomini, F. Cioffi, K. Broersen, V. Roviello, C. Riccardi, D. Montesarchio, D. Capasso, S.D. Gaetano, D. Musumeci, G.N. Roviello, Benzodifurans for biomedical applications: BZ4, a selective anti-proliferative and anti-amyloid lead compound, Future Med. Chem., 11 (2019) 285-302.
[12] Y. Wang, D.C. Latshaw, C.K. Hall, Aggregation of Aβ(17–36) in the Presence of Naturally Occurring Phenolic Inhibitors Using Coarse-Grained Simulations, Journal of Molecular Biology, 429 (2017) 3893-3908.
[13] E.A. Permyakov, M.H. Viet, C.-Y. Chen, C.-K. Hu, Y.-R. Chen, M.S. Li, Discovery of Dihydrochalcone as Potential Lead for Alzheimer's Disease: In Silico and In Vitro Study, PLoS ONE, 8 (2013) e79151.
[14] S.T. Ngo, M.S. Li, Curcumin Binds to Aβ1–40 Peptides and Fibrils Stronger Than Ibuprofen and Naproxen, The Journal of Physical Chemistry B, 116 (2012) 10165-10175.
[15] K.W. Bentley, The isoquinoline alkaloids, (1975) 259-348.
[16] I. Orhan, B. Özçelik, T. Karaoğlu, B. Şener, Antiviral and Antimicrobial Profiles of Selected Isoquinoline Alkaloids from Fumaria and Corydalis Species, Zeitschrift für Naturforschung C, 62 (2007) 19-26.
[17] S. Mehrzadi, I. Fatemi, M. Esmaeilizadeh, H. Ghaznavi, H. Kalantar, M. Goudarzi, Hepatoprotective effect of berberine against methotrexate induced liver toxicity in rats, Biomedicine & Pharmacotherapy, 97 (2018) 233-239.
[18] O.J. Patiño Ladino, L.E. Cuca Suárez, Isoquinoline alkaloids of Zanthoxylum quinduense (Rutaceae), Biochemical Systematics and Ecology, 38 (2010) 853-856.
[19] M.I.A. Kim, K.-H. Cho, M.-S. Shin, J.-M. Lee, H.-S. Cho, C.-J. Kim, D.-H. Shin, H.J. Yang, Berberine prevents nigrostriatal dopaminergic neuronal loss and suppresses hippocampal apoptosis in mice with Parkinson's disease, International Journal of Molecular Medicine, 33 (2014) 870-878.
[20] T. Ahmed, A.-u.-H. Gilani, M. Abdollahi, M. Daglia, S.F. Nabavi, S.M. Nabavi, Berberine and neurodegeneration: A review of literature, Pharmacological Reports, 67 (2015) 970-979.
[21] K.S. Shin, H.S. Choi, T.T. Zhao, K.H. Suh, I.H. Kwon, S.O. Choi, M.K. Lee, Neurotoxic effects of berberine on long-term l-DOPA administration in 6-hydroxydopamine-lesioned rat model of Parkinson's disease, Archives of Pharmacal Research, 36 (2013) 759-767.
[22] K. Rajasekhar, S. Samanta, V. Bagoband, N.A. Murugan, T. Govindaraju, Antioxidant Berberine-Derivative Inhibits Multifaceted Amyloid Toxicity, iScience, 23 (2020) 101005.
[23] K.-Y. Zee-Cheng, K.D. Paull, C.C. Cheng, Experimental antileukemic agents. Coralyne, analogs, and related compounds, Journal of Medicinal Chemistry, 17 (1974) 347-351.
[24] F. Xing, G. Song, J. Ren, J.B. Chaires, X. Qu, Molecular recognition of nucleic acids: Coralyne binds strongly to poly(A), FEBS Letters, 579 (2005) 5035-5039.
[25] G. Pi, P. Ren, J. Yu, R. Shi, Z. Yuan, C. Wang, Separation of sanguinarine and chelerythrine in Macleaya cordata (Willd) R. Br. based on methyl acrylate-co-divinylbenzene macroporous adsorbents, Journal of Chromatography A, 1192 (2008) 17-24.
[26] J. Dostál, M. Potáček, Quaternary benzo[c]phenanthridine alkaloids, Collection of Czechoslovak Chemical Communications, 55 (1990) 2840-2873.
[27] R. Zhang, X.W. Wang, J.Y. Zhu, L.L. Liu, Y.C. Liu, H. Zhu, Dietary sanguinarine affected immune response, digestive enzyme activity and intestinal microbiota of Koi carp (cryprinus carpiod), Aquaculture, 502 (2019) 72-79.
[28] C.M. Uhlar, A.S. Whitehead, Serum amyloid A, the major vertebrate acute-phase reactant, European Journal of Biochemistry, 265 (1999) 501-523.

[29] T. Miida, T. Yamada, U. Seino, M. Ito, Y. Fueki, A. Takahashi, K. Kosuge, S. Soda, O. Hanyu, K. Obayashi, O. Miyazaki, M. Okada, Serum amyloid A (SAA)-induced remodeling of CSF-HDL, Biochimica et Biophysica Acta (BBA) - Molecular and Cell Biology of Lipids, 1761 (2006) 424-433.
[30] H. Li, X. Xiang, H. Ren, L. Xu, L. Zhao, X. Chen, H. Long, Q. Wang, Q. Wu, Serum Amyloid A is a biomarker of severe Coronavirus Disease and poor prognosis, Journal of Infection, (2020).
[31] T. Wang, Z. Du, F. Zhu, Z. Cao, Y. An, Y. Gao, B. Jiang, Comorbidities and multi-organ injuries in the treatment of COVID-19, The Lancet, 395 (2020) e52.
[32] H.A. Rothan, S.N. Byrareddy, The epidemiology and pathogenesis of coronavirus disease (COVID-19) outbreak, Journal of Autoimmunity, 109 (2020) 102433.
[33] M. Costanzo, M.A.R. De Giglio, G.N. Roviello, SARS CoV-2: Recent Reports on Antiviral Therapies Based on Lopinavir/Ritonavir, Darunavir/Umifenovir, Hydroxychloroquine, Remdesivir, Favipiravir and Other Drugs for the Treatment of the New Coronavirus, Current medicinal chemistry, 27 (2020).
[34] V. Roviello, G.N. Roviello, Lower COVID-19 mortality in Italian forested areas suggests immunoprotection by Mediterranean plants, Environmental Chemistry Letters, (2020).
[35] C. Wiart, Lead compounds from medicinal plants for the treatment of neurodegenerative diseases, Academic Press, London, 2014.
[36] G. Brunhofer, A. Fallarero, D. Karlsson, A. Batista-Gonzalez, P. Shinde, C. Gopi Mohan, P. Vuorela, Exploration of natural compounds as sources of new bifunctional scaffolds targeting cholinesterases and beta amyloid aggregation: The case of chelerythrine, Bioorganic & Medicinal Chemistry, 20 (2012) 6669-6679.
[37] S.T. Ngo, M.S. Li, Top-leads from natural products for treatment of Alzheimer's disease: docking and molecular dynamics study, Molecular Simulation, 39 (2013) 279-291.
[38] K. Broersen, W. Jonckheere, J. Rozenski, A. Vandersteen, K. Pauwels, A. Pastore, F. Rousseau, J. Schymkowitz, A standardized and biocompatible preparation of aggregate-free amyloid beta peptide for biophysical and biological studies of Alzheimer's disease, Protein Engineering Design and Selection, 24 (2011) 743-750.
[39] M. Moccia, G.N. Roviello, E.M. Bucci, C. Pedone, M. Saviano, Synthesis of a l-lysine-based alternate alpha,epsilon-peptide: a novel linear polycation with nucleic acids-binding ability, Int J Pharm, 397 (2010) 179-183.
[40] G.N. Roviello, S.D. Gaetano, D. Capasso, A. Cesarani, E.M. Bucci, C. Pedone, Synthesis, spectroscopic studies and biological activity of a novel nucleopeptide with Moloney murine leukemia virus reverse transcriptase inhibitory activity, Amino Acids, 38 (2010) 1489-1496.
[41] G.N. Roviello, V. Roviello, I. Autiero, M. Saviano, Solid phase synthesis of TyrT, a thymine–tyrosine conjugate with poly(A) RNA-binding ability, RSC Advances, 6 (2016) 27607-27613.
[42] G.N. Roviello, C. Crescenzo, D. Capasso, S. Di Gaetano, S. Franco, E.M. Bucci, C. Pedone, Synthesis of a novel Fmoc-protected nucleoaminoacid for the solid phase assembly of 4-piperidyl glycine/l-arginine-containing nucleopeptides and preliminary RNA interaction studies, Amino Acids, 39 (2010) 795-800.
[43] G.N. Roviello, Novel insights into nucleoamino acids: biomolecular recognition and aggregation studies of a thymine-conjugated l-phenyl alanine, Amino Acids, 50 (2018) 933-941.
[44] M.A. Fik-Jaskółka, A.F. Mkrtchyan, A.S. Saghyan, R. Palumbo, A. Belter, L.A. Hayriyan, H. Simonyan, V. Roviello, G.N. Roviello, Spectroscopic and SEM evidences for G4-DNA binding by a synthetic alkyne-containing amino acid with anticancer activity, Spectrochimica Acta Part A: Molecular and Biomolecular Spectroscopy, 229 (2020) 117884.
[45] D. Musumeci, A. Mokhir, G.N. Roviello, Synthesis and nucleic acid binding evaluation of a thyminyl L-diaminobutanoic acid-based nucleopeptide, Bioorganic Chemistry, (2020) 103862.
[46] G. Oliviero, N. Borbone, J. Amato, S. D'Errico, A. Galeone, G. Piccialli, M. Varra, L. Mayol, Synthesis of quadruplex-forming tetra-end-linked oligonucleotides: effects of the linker size on quadruplex topology and stability, Biopolymers, 91 (2009) 466-477.
[47] A.S. Saghyan, H.M. Simonyan, S.G. Petrosyan, A.V. Geolchanyan, G.N. Roviello, D. Musumeci, V. Roviello, Thiophenyl-substituted triazolyl-thione l-alanine: asymmetric synthesis, aggregation and biological properties, Amino Acids, 46 (2014) 2325-2332.

[48] G.N. Roviello, M. Moccia, R. Sapio, M. Valente, E.M. Bucci, M. Castiglione, C. Pedone, G. Perretta, E. Benedetti, D. Musumeci, Synthesis, characterization and hybridization studies of new nucleo-gamma-peptides based on diaminobutyric acid, J Pept Sci, 12 (2006) 829-835.
[49] A. Carella, V. Roviello, R. Iannitti, R. Palumbo, S. La Manna, D. Marasco, M. Trifuoggi, R. Diana, G.N. Roviello, Evaluating the biological properties of synthetic 4-nitrophenyl functionalized benzofuran derivatives with telomeric DNA binding and antiproliferative activities, Int. J. Biol. Macromol., 121 (2019) 77-88.
[50] P. Krupa, P.D. Quoc Huy, M.S. Li, Properties of monomeric Aβ42 probed by different sampling methods and force fields: Role of energy components, The Journal of Chemical Physics, 151 (2019) 055101.
[51] M.J. Frisch, G.W. Trucks, H.B. Schlegel, G.E. Scuseria, M.A. Robb, J.R. Cheeseman, G. Scalmani, V. Barone, G.A. Petersson, H. Nakatsuji, X. Li, M. Caricato, A.V. Marenich, J. Bloino, B.G. Janesko, R. Gomperts, B. Mennucci, H.P. Hratchian, J.V. Ortiz, A.F. Izmaylov, J.L. Sonnenberg, Williams, F. Ding, F. Lipparini, F. Egidi, J. Goings, B. Peng, A. Petrone, T. Henderson, D. Ranasinghe, V.G. Zakrzewski, J. Gao, N. Rega, G. Zheng, W. Liang, M. Hada, M. Ehara, K. Toyota, R. Fukuda, J. Hasegawa, M. Ishida, T. Nakajima, Y. Honda, O. Kitao, H. Nakai, T. Vreven, K. Throssell, J.A. Montgomery Jr., J.E. Peralta, F. Ogliaro, M.J. Bearpark, J.J. Heyd, E.N. Brothers, K.N. Kudin, V.N. Staroverov, T.A. Keith, R. Kobayashi, J. Normand, K. Raghavachari, A.P. Rendell, J.C. Burant, S.S. Iyengar, J. Tomasi, M. Cossi, J.M. Millam, M. Klene, C. Adamo, R. Cammi, J.W. Ochterski, R.L. Martin, K. Morokuma, O. Farkas, J.B. Foresman, D.J. Fox, Gaussian 16 Rev. C.01, Wallingford, CT, 2016.
[52] A. Jakalian, D.B. Jack, C.I. Bayly, Fast, efficient generation of high-quality atomic charges. AM1-BCC model: II. Parameterization and validation, J Comput Chem, 23 (2002) 1623-1641.
[53] J. Wang, R.M. Wolf, J.W. Caldwell, P.A. Kollman, D.A. Case, Development and testing of a general amber force field, Journal of Computational Chemistry, 25 (2004) 1157-1174.
[54] G.M. Morris, R. Huey, W. Lindstrom, M.F. Sanner, R.K. Belew, D.S. Goodsell, A.J. Olson, AutoDock4 and AutoDockTools4: Automated docking with selective receptor flexibility, Journal of Computational Chemistry, 30 (2009) 2785-2791.
[55] N.T. Nguyen, T.H. Nguyen, T.N.H. Pham, N.T. Huy, M.V. Bay, M.Q. Pham, P.C. Nam, V.V. Vu, S.T. Ngo, Autodock Vina Adopts More Accurate Binding Poses but Autodock4 Forms Better Binding Affinity, Journal of Chemical Information and Modeling, 60 (2019) 204-211.
[56] J.A. Maier, C. Martinez, K. Kasavajhala, L. Wickstrom, K.E. Hauser, C. Simmerling, ff14SB: Improving the Accuracy of Protein Side Chain and Backbone Parameters from ff99SB, Journal of Chemical Theory and Computation, 11 (2015) 3696-3713.
[57] W.L. Jorgensen, J. Chandrasekhar, J.D. Madura, R.W. Impey, M.L. Klein, Comparison of simple potential functions for simulating liquid water, The Journal of Chemical Physics, 79 (1983) 926-935.
[58] C. Tian, K. Kasavajhala, K.A.A. Belfon, L. Raguette, H. Huang, A.N. Migues, J. Bickel, Y. Wang, J. Pincay, Q. Wu, C. Simmerling, ff19SB: Amino-Acid-Specific Protein Backbone Parameters Trained against Quantum Mechanics Energy Surfaces in Solution, Journal of Chemical Theory and Computation, 16 (2019) 528-552.
[59] S. Izadi, R. Anandakrishnan, A.V. Onufriev, Building Water Models: A Different Approach, The Journal of Physical Chemistry Letters, 5 (2014) 3863-3871.
[60] J.r. Weiser, P.S. Shenkin, W.C. Still, Approximate atomic surfaces from linear combinations of pairwise overlaps (LCPO), Journal of Computational Chemistry, 20 (1999) 217-230.
[61] W. Kabsch, C. Sander, Dictionary of protein secondary structure: Pattern recognition of hydrogen-bonded and geometrical features, Biopolymers, 22 (1983) 2577-2637.
[62] H.L. Nguyen, P. Krupa, N.M. Hai, H.Q. Linh, M.S. Li, Structure and Physicochemical Properties of the Aβ42 Tetramer: Multiscale Molecular Dynamics Simulations, The Journal of Physical Chemistry B, 123 (2019) 7253-7269.
[63] M.M. Picken, G.A. Herrera, Thioflavin T Stain: An Easier and More Sensitive Method for Amyloid Detection, (2012) 187-189.
[64] H.M. Sanders, R. Lust, J.K. Teller, Amyloid-beta peptide Aβp3-42 affects early aggregation of full-length Aβ1-42, Peptides, 30 (2009) 849-854.
[65] C. Di Natale, P.L. Scognamiglio, R. Cascella, C. Cecchi, A. Russo, M. Leone, A. Penco, A. Relini, L. Federici, A. Di Matteo, F. Chiti, L. Vitagliano, D. Marasco, Nucleophosmin contains amyloidogenic regions that are able to form toxic aggregates under physiological conditions, FASEB J, 29 (2015) 3689-3701.

[66] A. Monji, H. Utsumi, T. Ueda, T. Imoto, I. Yoshida, S. Hashioka, K.-i. Tashiro, N. Tashiro, The relationship between the aggregational state of the amyloid-β peptides and free radical generation by the peptides, Journal of Neurochemistry, 77 (2001) 1425-1432.
[67] B. Guivernau, J. Bonet, V. Valls-Comamala, M. Bosch-Morato, J.A. Godoy, N.C. Inestrosa, A. Peralvarez-Marin, X. Fernandez-Busquets, D. Andreu, B. Oliva, F.J. Munoz, Amyloid-beta Peptide Nitrotyrosination Stabilizes Oligomers and Enhances NMDAR-Mediated Toxicity, J Neurosci, 36 (2016) 11693-11703.
[68] S.A. Kotler, J.R. Brender, S. Vivekanandan, Y. Suzuki, K. Yamamoto, M. Monette, J. Krishnamoorthy, P. Walsh, M. Cauble, M.M. Holl, E.N. Marsh, A. Ramamoorthy, High-resolution NMR characterization of low abundance oligomers of amyloid-beta without purification, Sci Rep, 5 (2015) 11811.
[69] J. Guo, W. Sun, L. Li, F. Liu, W. Lu, Brazilin inhibits fibrillogenesis of human islet amyloid polypeptide, disassembles mature fibrils, and alleviates cytotoxicity, RSC Advances, 7 (2017) 43491-43501.
[70] B. Cheng, X. Liu, H. Gong, L. Huang, H. Chen, X. Zhang, C. Li, M. Yang, B. Ma, L. Jiao, L. Zheng, K. Huang, Coffee Components Inhibit Amyloid Formation of Human Islet Amyloid Polypeptide in Vitro: Possible Link between Coffee Consumption and Diabetes Mellitus, Journal of Agricultural and Food Chemistry, 59 (2011) 13147-13155.
[71] B. Cheng, H. Gong, X. Li, Y. Sun, X. Zhang, H. Chen, X. Liu, L. Zheng, K. Huang, Silibinin inhibits the toxic aggregation of human islet amyloid polypeptide, Biochemical and Biophysical Research Communications, 419 (2012) 495-499.
[72] F.L. Palhano, J. Lee, N.P. Grimster, J.W. Kelly, Toward the Molecular Mechanism(s) by Which EGCG Treatment Remodels Mature Amyloid Fibrils, Journal of the American Chemical Society, 135 (2013) 7503-7510.
[73] C. Di Natale, S. La Manna, C. Avitabile, D. Florio, G. Morelli, P.A. Netti, D. Marasco, Engineered β-hairpin scaffolds from human prion protein regions: Structural and functional investigations of aggregates, Bioorganic Chemistry, 96 (2020) 103594.
[74] C. Di Natale, S. La Manna, A.M. Malfitano, S. Di Somma, D. Florio, P.L. Scognamiglio, E. Novellino, P.A. Netti, D. Marasco, Structural insights into amyloid structures of the C-terminal region of nucleophosmin 1 in type A mutation of acute myeloid leukemia, Biochimica et Biophysica Acta (BBA) - Proteins and Proteomics, 1867 (2019) 637-644.
[75] D. Florio, A.M. Malfitano, S. Di Somma, C. Mugge, W. Weigand, G. Ferraro, I. Iacobucci, M. Monti, G. Morelli, A. Merlino, D. Marasco, Platinum(II) O,S Complexes Inhibit the Aggregation of Amyloid Model Systems, Int J Mol Sci, 20 (2019).
[76] Florio, Iacobucci, Ferraro, Mansour, Morelli, Monti, Merlino, Marasco, Role of the Metal Center in the Modulation of the Aggregation Process of Amyloid Model Systems by Square Planar Complexes Bearing 2-(2'-pyridyl)benzimidazole Ligands, Pharmaceuticals, 12 (2019) 154.
[77] P.L. Scognamiglio, C. Di Natale, M. Leone, R. Cascella, C. Cecchi, L. Lirussi, G. Antoniali, D. Riccardi, G. Morelli, G. Tell, F. Chiti, D. Marasco, Destabilisation, aggregation, toxicity and cytosolic mislocalisation of nucleophosmin regions associated with acute myeloid leukemia, Oncotarget, 7 (2016) 59129-59143.
[78] S. La Manna, P.L. Scognamiglio, V. Roviello, F. Borbone, D. Florio, C. Di Natale, A. Bigi, C. Cecchi, R. Cascella, C. Giannini, T. Sibillano, E. Novellino, D. Marasco, The acute myeloid leukemia-associated Nucleophosmin 1 gene mutations dictate amyloidogenicity of the C-terminal domain, FEBS J., (2019).
[79] M. Poletto, M.C. Malfatti, D. Dorjsuren, P.L. Scognamiglio, D. Marasco, C. Vascotto, A. Jadhav, D.J. Maloney, D.M. Wilson, 3rd, A. Simeonov, G. Tell, Inhibitors of the apurinic/apyrimidinic endonuclease 1 (APE1)/nucleophosmin (NPM1) interaction that display anti-tumor properties, Molecular carcinogenesis, 55 (2016) 688-704.
[80] M. Chu, X. Chen, J. Wang, L. Guo, Q. Wang, Z. Gao, J. Kang, M. Zhang, J. Feng, Q. Guo, B. Li, C. Zhang, X. Guo, Z. Chu, Y. Wang, Polypharmacology of Berberine Based on Multi-Target Binding Motifs, Frontiers in Pharmacology, 9 (2018).
[81] B.-k. Shin, S. Saxena, Substantial Contribution of the Two Imidazole Rings of the His13−His14 Dyad to Cu(II) Binding in Amyloid-β(1−16) at Physiological pH and Its Significance, The Journal of Physical Chemistry A, 115 (2011) 9590-9602.
[82] S.L. Bernstein, N.F. Dupuis, N.D. Lazo, T. Wyttenbach, M.M. Condron, G. Bitan, D.B. Teplow, J.-E. Shea, B.T. Ruotolo, C.V. Robinson, M.T. Bowers, Amyloid-β protein oligomerization and the importance of tetramers and dodecamers in the aetiology of Alzheimer's disease, Nature Chemistry, 1 (2009) 326-331.

[83] D.M. Walsh, D.M. Hartley, Y. Kusumoto, Y. Fezoui, M.M. Condron, A. Lomakin, G.B. Benedek, D.J. Selkoe, D.B. Teplow, Amyloid β-Protein Fibrillogenesis, Journal of Biological Chemistry, 274 (1999) 25945-25952.
[84] S. Zhang, K. Iwata, M.J. Lachenmann, J.W. Peng, S. Li, E.R. Stimson, Y.a. Lu, A.M. Felix, J.E. Maggio, J.P. Lee, The Alzheimer's Peptide Aβ Adopts a Collapsed Coil Structure in Water, Journal of Structural Biology, 130 (2000) 130-141.
[85] M.G. Krone, L. Hua, P. Soto, R. Zhou, B.J. Berne, J.-E. Shea, Role of Water in Mediating the Assembly of Alzheimer Amyloid-β Aβ16−22 Protofilaments, Journal of the American Chemical Society, 130 (2008) 11066-11072.
[86] J. Hu, H. Sun, H. Hao, Q. Zheng, Prediction of fibril formation by early-stage amyloid peptide aggregation, Journal of Pharmaceutical Analysis, 10 (2020) 194-199.
[87] S. Giorgetti, C. Greco, P. Tortora, F. Aprile, Targeting Amyloid Aggregation: An Overview of Strategies and Mechanisms, International Journal of Molecular Sciences, 19 (2018) 2677.
[88] T.T.M. Thu, N.T. Co, L.A. Tu, M.S. Li, Aggregation rate of amyloid beta peptide is controlled by beta-content in monomeric state, The Journal of Chemical Physics, 150 (2019) 225101.
[89] T. Zhang, J. Loschwitz, B. Strodel, L. Nagel-Steger, D. Willbold, Interference with Amyloid-β Nucleation by Transient Ligand Interaction, Molecules, 24 (2019) 2129.
[90] A.J. Modler, K. Gast, G. Lutsch, G. Damaschun, Assembly of Amyloid Protofibrils via Critical Oligomers—A Novel Pathway of Amyloid Formation, Journal of Molecular Biology, 325 (2003) 135-148.

# Highlights

- We compared the effects of three isoquinoline alkaloids on β-amyloid aggregation
- Sanguinarine and chelerythrine showed inhibitory effects on $A\beta_{1-42}$ aggregation
- Coralyne significantly increased propensity for $A\beta_{1-42}$ to aggregate
- Molecular dynamics suggested the alkaloid ability to affect β-content of $A\beta_{1-42}$

**Declaration of interests**

☒ The authors declare that they have no known competing financial interests or personal relationships that could have appeared to influence the work reported in this paper.

☐The authors declare the following financial interests/personal relationships which may be considered as potential competing interests: